Desalination and Water Treatment
www.deswater.com
doi: 10.1080/19443994.2016.1175969

57 (2016) 27726–27740
December

Taylor & Francis
Taylor & Francis Group

Adsorption of liquid fuel dimethyl amino ethyl azide from dilute aqueous solution on activated carbon prepared from walnut shell

Shahram Ghanbari Pakdehi*, Fatemeh Rezaei

Faculty of Chemical Engineering, Malek Ashtar University of Technology, P.O. Box 16765/3454, Tehran, Iran, Tel. +98 021 61112203; Fax: +98 021 61112308; email: sh_ghanbari73@yahoo.com (S.G. Pakdehi)

Received 20 October 2015; Accepted 2 April 2016

ABSTRACT

Dimethyl amino ethyl azide (DMAZ) is a non-carcinogenic liquid fuel in space programs. Low concentrations of DMAZ should be separated from dilute aqueous solution to prevent the environmental pollution. Activated carbon, prepared from walnut shell through zinc chloride activation, was characterized and assessed to remove DMAZ from dilute aqueous solutions. At initial concentration of 500 ppm of DMAZ, the optimum conditions were obtained as pH 10, agitation speed of 100 rpm, and adsorbent dosage of 0.29 g. Under the optimized conditions, the removal percentage was obtained as 85.95%. Adsorption data for DMAZ uptake by the activated carbon was analyzed according to Langmuir, Freundlich, Tempkin, and Dubinin–Radushkevich (D–R) adsorption models. The results indicated that the Freundlich model agreed well with the isotherm data. Among the pseudo-first-order, pseudo-second-order, Elovich, and intraparticle diffusion kinetic models, the kinetic process can be described by a pseudo-second-order rate equation very well. It was found that the activated carbon prepared from walnut shell could be considered as an appropriate adsorbent for DMAZ in dilute aqueous solution.

Keywords: DMAZ; Adsorption; Walnut shell; Isotherms; Kinetic

1. Introduction

Liquid fuels have been consumed in rocket engines in space industries since 1949. Among the liquid fuels, hydrazine group (containing anhydrous hydrazine, monomethyl hydrazine, and unsymmetrical dimethyl hydrazine) has been consumed extensively. However, all members of this group are carcinogenic [1,2]. Scientists and engineers pursue safe and high-performance liquid fuels; consequently, they have introduced dimethyl amino ethyl azide (DMAZ) as an appropriate replacement for hydrazine liquid fuels in space industries [1,3,4]. DMAZ is a non-carcinogenic liquid fuel, but it is toxic like almost chemicals [5].

DMAZ is colorless with a pungent odor. Moreover, DMAZ is chemically classified in organic azide group, that is, unstable and potentially explosive. However, it is more stable than other organic azides due to its semi-ring structure [6]. The structure of DMAZ is shown in Fig. 1.

DMAZ is produced from the reaction between dimethyl amino ethyl chloride and sodium azide [7,8]. The final product is concentrated through a zeolite membrane. Water passes through the membrane (as permeate) and DMAZ remains in the retentive phase [9,10]. For low concentrations of DMAZ in the

*Corresponding author.

Fig. 1. Semi-ring structure (left) and linear structure (right) of DMAZ molecule [6].

permeate phase (in ppm), the separation or recovery of DMAZ is not economically feasible [11]. Thus, it is wasted to surface waters. DMAZ, as almost all synthetic chemicals, has unfavorable effects on the environment and especially on surface waters. Therefore, the removal of DMAZ in waste effluents is an essential environmental issue of concern.

Very low concentrations of a pollutant may be removed from wastewater through several methods [12–15]. Among them, adsorption is very appropriate since it is simple and easy to control [16–20]. Activated carbon in particular is the most conventional adsorbent, in treating low concentrations of organic pollutants [21,22]. Activated carbon has a high specific surface area with high porosity. It is produced from many carbon chemicals. However, the final properties of this carbon significantly depend on the nature of starting materials [23]. Consuming effective commercial activated carbons based on relatively expensive starting materials is not justified for most pollution control applications; therefore, it is important to examine the feasibility of consuming cheaper raw materials to prepare activated carbon. Numerous successful attempts have been made to develop activated carbons from various types of agricultural solid wastes such as hen feather [24], rice husk [25], rubber-wood sawdust [26], de-oiled soya [27], oil palm shell [28], coir pith [29], coconut husk [30], and bottom ash [31].

Walnut is relatively expensive all over the world and its shell has no value and is wasted. The outstanding approach in this study is the conversion of walnut shell into activated carbon for DMAZ removal from very dilute solution. Here, walnut shell was chosen as a source of activated carbon. DMAZ was adsorbed on this activated carbon. Design of experiments (DOE) method was used to study the effective parameters on the adsorption efficiency and the adsorption isotherms were studied to determine the adsorbent capacity. The kinetic of DMAZ adsorption on the activated carbon was studied as well. The kinetic study will provide useful information for scaling up the process.

2. Experimental

2.1. Chemicals

Walnut shell (Fig. 2), as a priceless starting material, was collected from walnut gardens of Touiserkan (Iran), washed with double distilled water four times for dirt and dust particles removal and dried up to 110°C for 2 h. Zinc chloride ($ZnCl_2$) was added with heating (up to 100°C) to form a brown paste. The produced paste was then placed in an electrical furnace and heated at 500°C for 30 min, then cooled down gradually, neutralized by a dilute solution of HCl, and washed with distilled water and dried again at 110°C. The final product was ground and passed through a No. 100 sieve. To avoid humidification, the activated carbon was maintained in a desiccator.

DMAZ (purity >99.99 wt.%) was purchased from 3M Company (USA). The dilute aqueous solutions of hydrochloric acid and sodium hydroxide were consumed for pH adjustment.

Fig. 2. A photo of walnut shell (from gardens of Touiserkan, Iran)-left side; and the resultant activated carbon-right side.

2.2. Characterization of the activated carbon

Surface characterization analyses were run by N_2 adsorption at –196°C using adsorption apparatus (Covantocrom, model: NOVA 2000, USA). The BET surface areas (S_{BET}), micropore areas (S_{micro}), and total micropore volumes (V_{total}) were calculated through N_2 adsorption isotherms.

Surface morphology of the activated carbon was studied by VEGA3 SEM (model TESCAN). Transmission electron microscope (model JEM 2010) was used to examine the microstructure of the activated carbon. For TEM measurement, the powder samples were dispersed in ethanol and dried on a carbon film with multiple holes on a Cu grid for measurements.

The IR spectra (by Perkin–Elmer 1600 FT-IR spectrophotometer) were obtained both before and after DMAZ adsorption on this activated carbon.

2.3. Analysis

UV–visible spectrophotometer (Hitachi model 3101, Japan) was used to determine the DMAZ concentration in aqueous solution. For this purpose, DMAZ solutions were prepared with various low concentrations. The amounts of light absorption vs. different DMAZ concentrations were recorded and a calibration curve was prepared where, λ_{max} was 283 nm for DMAZ.

The batch technique was applied in the adsorption experiments. The weight of this activated carbon was measured by a 0.001 g precision digital analytical balance (model WT2003N, Canada) and poured into the Erlenmeyer flask. Next, various concentrations of DMAZ solution were poured to the flask which was then put in a shaker (Thermo Scientific, model: 420) equipped with a water bath for temperature control. Samples at different times were passed through a filter paper and then analyzed.

2.4. Effective parameters and DOE

At constant particle size of the activated carbon and constant initial concentration of DMAZ in feed, interaction among the effective parameters and optimization were assessed through DOE. DOE is an approach in solving problems involved in collection of data that would support valid, defensible, and supportable conclusions [32]. Design-Expert 7.1.3, as a proper software, was used for this purpose. Preliminary tests indicated that the adsorbent dosage, pH, and agitation speed were the effective parameters. The adsorbent dosage was assessed at two levels of 0.25–0.5 g. pH values were studied at three levels of four (acid medium), 7 (neutral medium), and 10 (basic medium). Agitation speed was assessed at two levels of 50–100 rpm. The general factorial method with three qualitative factors and one answer or target (removal percentage) dictated 12 experiments. The removal percentage was calculated through Eq. (1):

$$\text{DMAZ adsorption } (\%) = (A_o - A)/A_o \times 100 \quad (1)$$

where A_o is the initial liquid-phase concentration of DMAZ, A is the experimental concentration in the solution at equilibrium state.

2.5. Adsorption isotherms

The four equilibrium models (Langmuir, Freundlich, Tempkin, and Dubinin–Radushkevich (D–R)) were adopted here to assess the adsorption isotherms.

The Langmuir isotherm has been reported in most of adsorption processes [33]. It considers that the adsorption energy of each molecule is the same, independent from the material surface. The adsorption occurs on the same sites and there are no interactions between the molecules. In other words, Langmuir isotherm is a single layer adsorption. The mathematical form of Langmuir isotherm is [34]:

$$\frac{1}{q_e} = \frac{1}{bQ_mC_e} + \frac{1}{Q_m} \quad (2)$$

where C_e is the concentration of liquid phase at equilibrium state, q_e is the amount of sorbate adsorbed per unit weight of adsorbent, Q_m and b are the Langmuir constants related to the monolayer sorption capacity and equilibrium constant, respectively.

The Freundlich isotherm provides an empirical model between sorption capacity and equilibrium concentration of the adsorbent. Unlike the Langmuir isotherm, the surface of adsorbent is non-homogeneous and the active sites are of different energies. The Freundlich isotherm is used more extensively than the Langmuir relationship. However, it provides no information on monolayer adsorption in comparison to Langmuir. The Linear form of this model is [35]:

$$\log q_e = \log K_F + \frac{1}{n}\log C_e \quad (3)$$

where q_e is the amount of DMAZ adsorbed at equilibrium state, C_e is the equilibrium concentration of

DMAZ in solution, and K_F and $1/n$ are the Freundlich constants which correspond to the adsorption capacity and adsorption intensity, respectively.

Regarding Tempkin isotherm, assumed that a drop in adsorption heat is linear rather than logarithmic as implied in the Freundlich equation. The heat of adsorption for all molecules at each layer would decrease linearly with coverage due to adsorbate/adsorbent interaction. The linear form of the Tempkin isotherm is expressed as [36]:

$$q_e = K_T \ln A_T + K_T \ln C_e \tag{4}$$

where C_e is the concentration of DMAZ at equilibrium state, q_e is the amount of DMAZ adsorbed at equilibrium per unit weight of the adsorbent, K_T is related to the heat of adsorption, and A_T is the equilibrium binding constant.

The Dubinin–Radushkevich (D–R) model was applied in estimating the porosity, apparent free energy, and characteristic of adsorption. In the D–R isotherm, it is not assumed a homogeneous surface or constant adsorption potential. The linear form of the D–R isotherm is presented as [13,37]:

$$\ln q_e = \ln q_s - B_{D-R}\varepsilon^2 \tag{5}$$

where q_e is the amount of DMAZ adsorbed at equilibrium, q_s is the theoretical monolayer saturation capacity, B_{D-R} is the D–R model constant, and ε is the Polanyi potential equal to $\varepsilon = RT \ln(1 + (1/C_e))$ [13]. R is the universal gas constant, T is the temperature, and C_e is the equilibrium concentration of DMAZ in solution.

2.6. Adsorption kinetics

Adsorption kinetics is important since it controls the efficiency of the process. In kinetic models, the adsorbate uptake rate is correlated to its bulk concentration. Experiments were performed in order to understand the kinetics of DMAZ removal by the activated carbon. To analyze the sorption rate, the kinetic data were modeled in pseudo-first-order, pseudo-second-order equations, Elovich kinetic, and intraparticle diffusion correlations [38–41]:

The pseudo-first-order:

$$\frac{dq_t}{dt} = k_1(q_e - q_t) \tag{6}$$

For boundary conditions $t = 0$ to $t = t$ and correspondingly $q_t = 0$ to $q_t = q_t$; the integrated form of this equation is:

$$\log(q_e - q_t) = \log(q_e) - \frac{k_1}{2.303}t \tag{7}$$

The pseudo-second-order equation:

$$\frac{dq_t}{dt} = k_2(q_e - q_t)^2 \tag{8}$$

Applying the boundary conditions as stated before, the integrated form of this equation is:

$$\frac{t}{q_t} = \frac{1}{k_2 q_e^2} + \frac{1}{q_e}t \tag{9}$$

where q_t and q_e are the amounts of DMAZ adsorbed at time t and at equilibrium, respectively. k_1 and k_2 are the rate constants of pseudo-first-order and pseudo-second-order adsorptions kinetics, respectively.

The Elovich equation:

$$\frac{dq_t}{dt} = \alpha \exp(-\beta q_t) \tag{10}$$

where α is the initial adsorption rate and β is the adsorption constant related to the extent of the surface coverage and activation energy for chemisorption. Eq. (10) is simplified by assuming $\alpha\beta > t$ and by applying the boundary conditions $t = 0$ to $t = t$ and correspondingly $q_t = 0$ to $q_t = q_t$, as presented by Eq. (11):

$$q_t = \frac{1}{\beta}\ln(\alpha\beta) + \frac{1}{\beta}\ln t \tag{11}$$

Intraparticle diffusion model:

The intraparticle diffusion model is expressed as:

$$q_t = k_3 t^{0.5} + j \tag{12}$$

where the plot of q_t vs. $t^{0.5}$ will be a straight line if the model is corrected by k_3 slope.

3. Results and discussion

3.1. Characterization results

It is observed that the activated carbon has a structure of micromesoporous mixture with a significantly high BET surface area of 1,480 $m^2\ g^{-1}$; therefore, it can be deduced that it may adsorb both small water molecules and large DMAZ molecules (Table 1). The BET surface area, pore volume, and average pore diameter

Table 1
Characteristics of the activated carbon before and after adsorption

Surface characteristics parameters of the activated carbon	Before adsorption	After adsorption
BET surface area ($m^2\ g^{-1}$)		
S_{BET}	1,480	1,453
S_{micro}	888	872
S_{meso}	592	581
Pore volume ($cm^3\ g^{-1}$)		
V_{total}	0.805	0.601
V_{micro}	0.467	0.349
V_{meso}	0.338	0.252
Average pore diameter (nm)	3.2	2.9

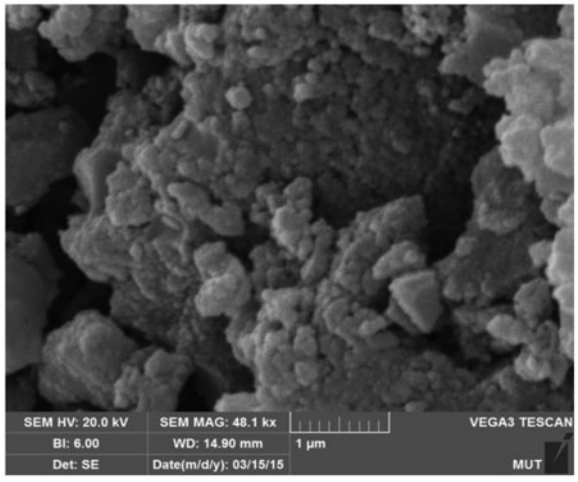

Fig. 3a. SEM image of activated carbon before the adsorption of DMAZ.

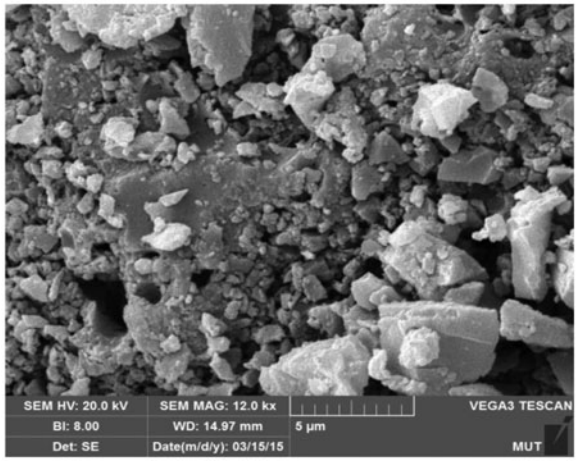

Fig. 3b. SEM image of activated carbon after the adsorption of DMAZ.

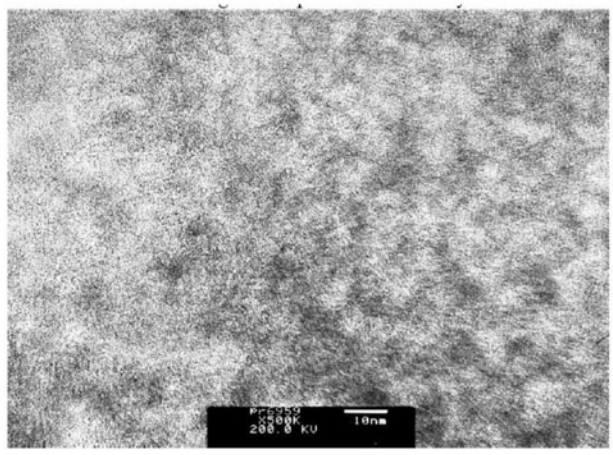

Fig. 4. TEM of the activated carbon prepared from walnut shell before or after the adsorption process.

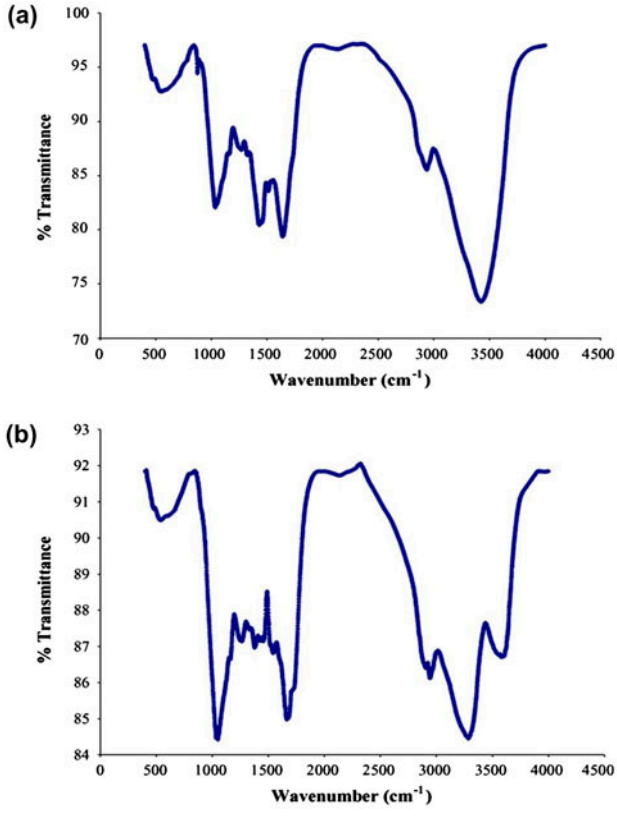

Fig. 5. The FT-IR spectra of activated carbon produced from walnut shell (a) before DMAZ adsorption and (b) after DMAZ adsorption.

for the activated carbon after adsorption are tabulated in this table. The results reveal that adsorption of DMAZ reduces BET surface area and pore volume, causing the average pore diameter to become smaller.

Table 2
The FT-IR spectral characteristics of activated carbon produced from walnut shell before and after DMAZ adsorption

IR peak	Before adsorption (cm^{-1})	After adsorption (cm^{-1})	Assignment
1	–	3,650	–NH stretching from amine salt
2	3,406	3,274	Bonded –OH group, –NH stretching,
3	2,928	2,936	Aliphatic C–H group
4	–	2,398	$–N_3$ group
5	1,635	1,662	C=C stretching
6	1,507	1,536	Secondary amine group
7	–	1,380	Tertiary amine group
8	1,421	1,372	Carboxyl group
9	1,317	1,320	Symmetric bending of CH_3, –CN stretching
10	1,243	1,245	–CN stretching
11	1,140	1,144	C–O stretching of ether group
12	1,029	1,031	–C–C– group
13	873	895	–C–C– group

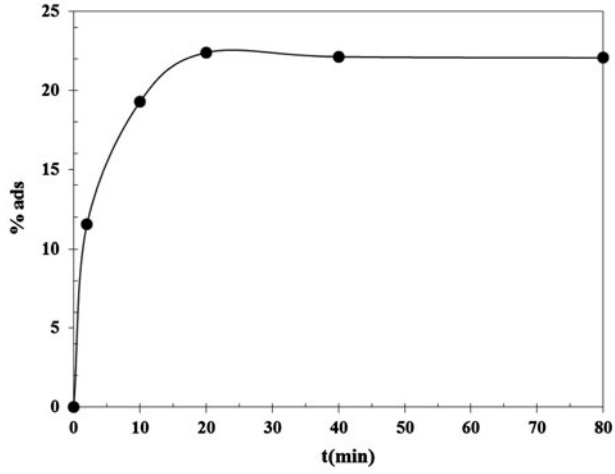

Fig. 6. The time dependency of DMAZ adsorption percent on the activated carbon ($C_{0,DMAZ}$ = 500 ppm, $m_{adsorbent}$ = 0.25 g, ω = 50 rpm, pH 10).

Surface morphology of the activated carbon is shown in Figs. 3a and 3b. Fig. 3a is the surface of the adsorbent before the adsorption and Fig. 3b after the adsorption. Unsymmetrical distribution of pores is observed in the adsorbent, as well as the porosity and the adsorption of activated carbon.

In the TEM image in Fig. 4, the carbon frame in the sample is visualized as black particles and the pores are shown as white areas. Both the mesopores and micropores are present in this activated carbon. Since the adsorption process occurs at low temperatures, there is no detectable difference in the activated carbon in TEM image before and after the adsorption process.

Characterization of the adsorbent was investigated by FT-IR spectral (Fig. 5(a) and (b)). The functional groups before (a) and after (b) adsorption on the activated carbon and the corresponding infrared absorption bands are tabulated in Table 2. In IR spectra

Table 3
The results of design of experiments (DOE) for DMAZ removal from dilute aqueous solution with the activated carbon

Run (#)	*A*: dosage of adsorbent (g)	*B*: pH	*C*: ω (rpm)	Response: DMAZ removal (%)
1	0.25	4	50	86.5
2	0.5	4	50	95.65
3	0.25	7	50	79.5
4	0.5	7	50	95.2
5	0.25	10	50	85.05
6	0.5	10	50	95.5
7	0.25	4	100	77.25
8	0.5	4	100	85.6
9	0.25	7	100	84.5
10	0.5	7	100	99
11	0.25	10	100	84.3
12	0.5	10	100	89.4

Table 4
The results of ANOVA analysis for the design of experiments

Source	Sum of squares	df	Mean squares	*F*-value	*p*-value prob. > *F*	
Model	388.54	4	97.13	5.18	0.0293	Significant
A = dosage of adsorbent	333.38	1	333.38	17.77	0.0040	
B = pH	10.70	1	10.70	0.57	0.4749	
C = ω	25.09	1	25.09	1.34	0.2855	
B × *C*	19.38	1	19.38	1.03	0.3433	
Residual	131.33	7	18.76			
Cor total	519.88	11				

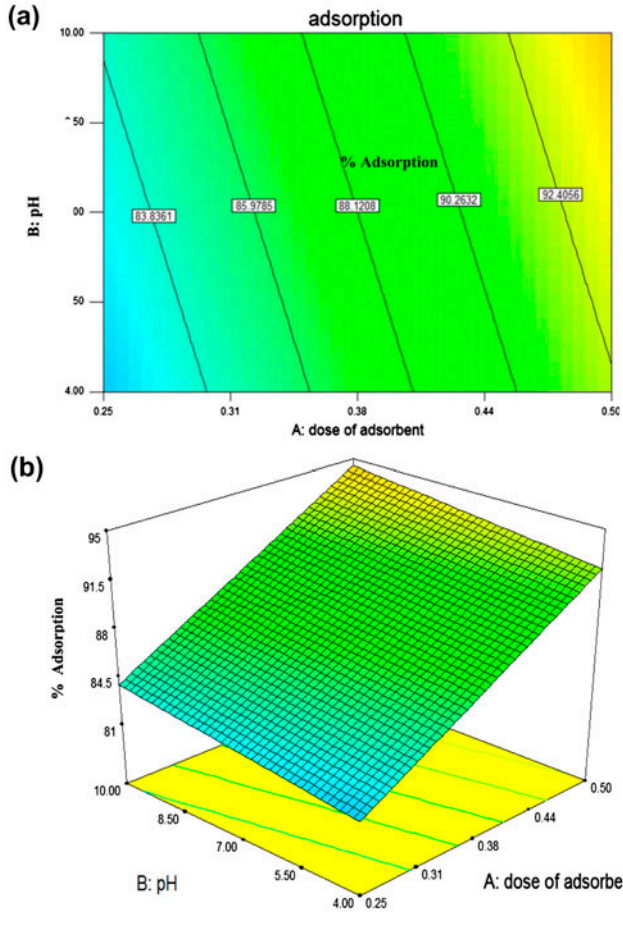

Fig. 7. Adsorption percentage vs. adsorbent dosage and pH in 2-dimensional diagram (a) and 3-dimensional diagram (b).

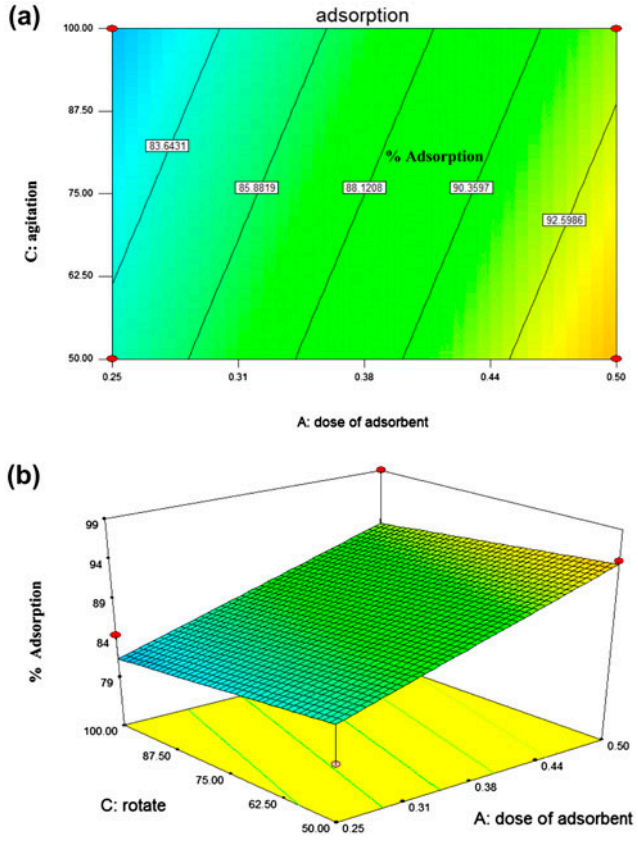

Fig. 8. Adsorption percentage vs. adsorbent dosage and agitation speed in 2-dimensional diagram (a) and 3-dimensional diagram (b).

taken before and after DMAZ adsorption, it is clear that the functional groups appeared approximately at the same frequencies. There are more peaks in the spectrum taken after DMAZ adsorption which refer to DMAZ molecules. Hence, increasing transmittance and extra peaks arising from DMAZ molecules that have entered the structure indicate DMAZ adsorption from aqueous solution by the activated carbon. After adsorption, the peak at 3,650 cm^{-1} indicates the existence of –NH stretching from amine salts. The azide type $-N_3$ peak appears at 2,398 cm^{-1} in the spectrum as well. Moreover, the peak at 1,380 cm^{-1} reveals the existence of tertiary amine group in DMAZ.

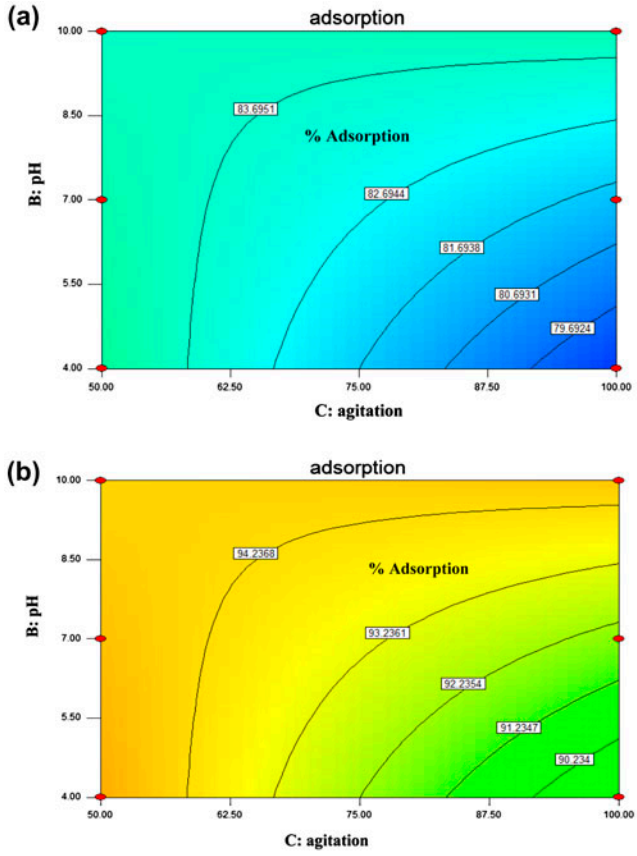

Fig. 9. Interactive effects of pH and agitation speed on adsorption at two levels of the adsorbent dosage (0.25 g (a) and 0.5 g (b)) in a 2-dimensional form.

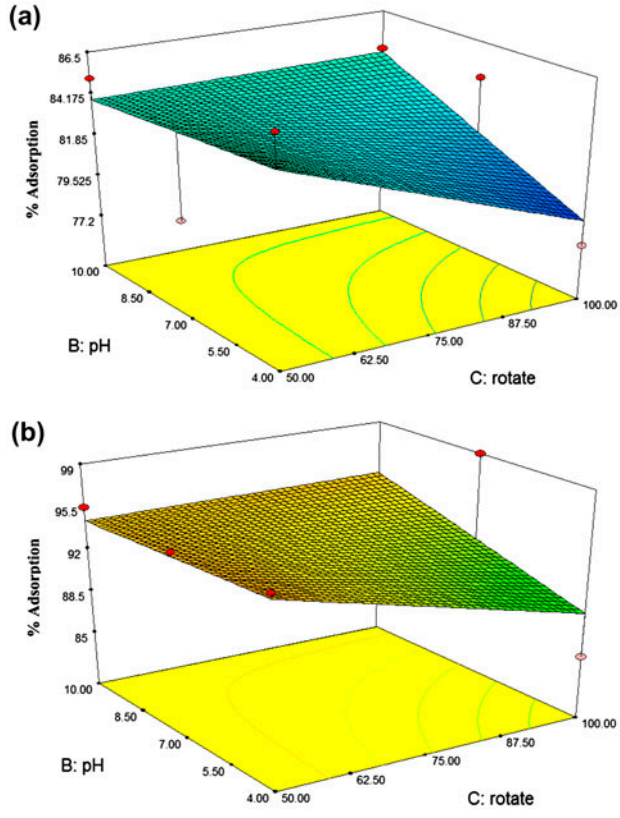

Fig. 10. Interactive effects of pH and agitation speed on adsorption at two levels of the adsorbent dosage (0.25 g (a) and 0.5 g (b)) in 3-dimensional form.

3.2. The parameters' optimization by DOE

The result of DMAZ adsorption on the activated carbon as a function of contact time is presented in Fig. 6. As observed, adsorption of DMAZ will become constant after 30 min, and is considered as equilibrium time to be applied in next experiments.

At equilibrium time of 30 min, DOE was conducted in order to assess the changes and interaction in parameters. In all experiments in optimization section, the initial concentration of DMAZ, contact time, the particle size of adsorbent, and the temperature were maintained constant at 500 ppm, 30 min, 100 mesh, and 25°C, respectively. Table 3 shows the results for the DOE.

The analysis of variance (ANOVA) is tabulated in Table 4 for the general factorial. In this model, the interaction among the adsorbent dosage (A), pH (B), and agitation speed (C) is not considered due to low *p*-value. As observed in Table 4, the amount of 0.0293 for *p*-value is a good confirmation for the suggested model (the *p*-value of the model should be less than 0.05 [42]). The following equation represents the interactive effect:

$$\text{Adsorption } (\%) = 84.8417 + 42.1667 \times A - 1.17083 \times B - 0.20308 \times C + 0.2075 \times B \times C \quad (13)$$

As observed here, dosage of adsorbent has the greatest influence.

The removal percentage on the basis of pH and the adsorbent dosage is shown in Fig. 7(a) and (b), where the removal percentage increases with an increase in the adsorbent dosage at constant pH and an increase in pH at constant adsorbent dosage.

This system leads to an increase in adsorption percentage with an increase in adsorbent dosage at constant agitation speed. It is also true for a reduction in agitation speed at constant adsorbent dosage (Fig. 8(a) and (b)).

As it is shown in Figs. 7 and 8, since the interaction between adsorbent dosage and both pH and

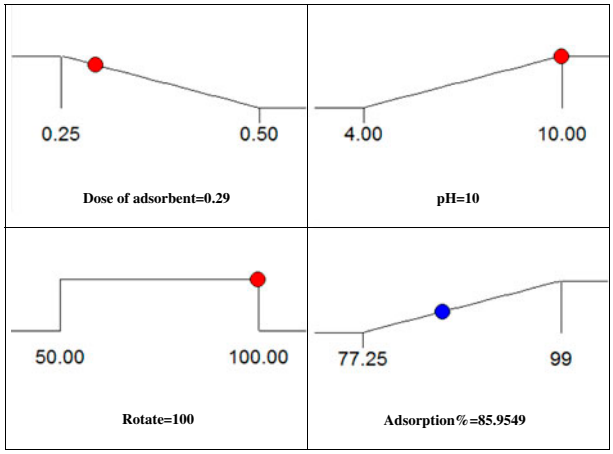

Fig. 11. The optimized condition according to the software calculations.

agitation speed is ignored, the equivalent level lines are straight. The interactive effect of pH and agitation speed for constant adsorbent dosage at two levels (0.25–0.5 g) is shown in Fig. 9. This interaction is observed in upper and lower limits of the adsorbent dosage. The equivalent level lines are the same for all dosages, hence, an increase in pH and adsorbent dosage enhances the removal percentage. At lower pH values, an increase in agitation speed decreases the removal percentage, while, at higher pH values, the lines will remain relatively constant and an increase in agitation speed would not have an effect on the removal percentage. The three-dimensional illustrations in Fig. 10 confirm this explanation.

An increase in the adsorbent dosage leads to a rise in adsorption and this is due to an increase in active sites available for adsorbed molecules of DMAZ. The vigorous agitation leads to a reduction in the boundary layer thickness around the adsorbent, therefore an increase in the mass transfer or adsorption [27,43,44]. However, in this system, pH and agitation speed have interactive effects. According to the Figs. 9 and 10, an increase or a decrease in both pH and agitation speed (specially increasing in both) leads to an increase in removal percentage. This is due to the basicity of DMAZ (pH for DMAZ is 9–10). The pH of solution is decreased by HCl solution. At lower pH values, the concentration of H^+ ion is more than that of higher pH values. Due to the smaller size of H^+ and its higher activity in relation to DMAZ molecules, agitation speed is appropriate for H^+, hence, the H^+ ion is adsorbed more than DMAZ. That is, the removal percentage decreases. At higher pH values (pH > 9), the equivalence level lines become flat and an increase in agitation speed almost increases the removal percentage.

In optimizing the effective parameters, the adsorbent dosage should be minimized. The energy consumption for mixer is negligible at lab scale, therefore, the agitation speed (ω) was considered in the studied interval. The pH of the solution should be maximized up to natural pH of DMAZ solution (pH 10). The objective of optimization is to obtain the maximum DMAZ removal from a given dilute solution. According to the software calculations, the optimum conditions are: pH 10, ω = 100 rpm, and the adsorbent dosage = 0.29 g. Under the optimized conditions, the removal percentage was obtained as 85.95% (Fig. 11). The experiments were run at the optimized conditions, revealed an adsorption percentage of 85.12.

3.3. The adsorption isotherms

The isotherm parameters of Langmuir, Freundlich, Tempkin, and D–R models for activated carbon prepared from walnut shell are tabulated in Table 5 and shown in Fig. 12. The value of correlation coefficient (R^2) was higher for Freundlich isotherm than that of the Langmuir, Tempkin, and D–R isotherms. This represents the fact that Freundlich isotherm is useful in explaining the adsorption from the solution on the current adsorbent. In other words, DMAZ adsorption occurs on the activated carbon in multilayer mode with non-homogeneous heat of adsorption and as internal bonds on non-homogeneous surface of the adsorbent. The stronger adsorption sites are firstly occupied until adsorption energy is reduced exponentially and the adsorption process is completed. Freundlich isotherm is used extensively in the non-homogeneous active sites especially for organic

Table 5
Parameters of Langmuir, Freundlich, Tempkin, and Dubinin–Radushkevich (D–R) isotherm models

Isotherm	Langmuir	Freundlich	D–R	Tempkin
R^2	0.8996	0.9627	0.5698	0.804
Constants	b = 0.1019	n = 1.8744	$B_{D–R}$ = 0.0000009	K_t = 170.58
	Q_m = 166.67	K_f = 18.433	q_s = 8.7373	A_t = 0.3481

compounds [45–49]. The range of 0–1 for slope $1/n$ represents the amount of adsorption or surface nonhomogenity. The $1/n$ approaching zero means higher nonhomogenity, while $1/n$ approaching 1 indicates the chemical adsorption [50].

3.4. Comparison of activated carbon from walnut shell with other adsorbents

The value of adsorption capacity is of importance in identifying the sorbent with the highest capacity and useful in consideration scale-up. A comparison of the adsorbent capacity of activated carbon from walnut shell with other sorbents is difficult due to the varying experimental conditions applied in such studies; however, the activated carbon from walnut shell in this study has a good adsorption capacity in comparison with other sorbent (Table 6).

3.5. Adsorption kinetics

The results of pseudo-first-order, pseudo-second-order, and Elovich kinetic models with correlation coefficients are tabulated in Table 7 and the related diagrams in Fig. 13. The correlation coefficient (R^2) for the pseudo-second-order equation was 0.9993. This coefficient strongly suggests that the sorption of DMAZ on the activated carbon is represented by a pseudo-second-order rate process in an appropriate manner.

3.6. Breakthrough time curve

In a batch adsorption system, breakthrough time is usually expressed in terms of DMAZ concentration in solution at each time over initial concentration of DMAZ ratio as a function of time at a given mass of the adsorbent [52]. The area under the breakthrough curve can be applied in finding the total adsorbed DMAZ quantity. The results from batch adsorption can be developed into an adsorption column [52] which in turn can be applied in column design. The breakthrough time is defined as the phenomenon when DMAZ concentration in the batch is about 3–5% of the initial concentration of DMAZ [53]. Under the optimized conditions (pH 10, ω = 100 rpm, the adsorbent dosage = 0.29 g), the breakthrough time curve is 500 ppm of initial concentration of DMAZ (Fig. 14). The effect of various initial concentrations of DMAZ on the breakthrough curve was assessed as well. Lower concentration of DMAZ will obviously reduce the breakthrough time. At initial concentrations lower

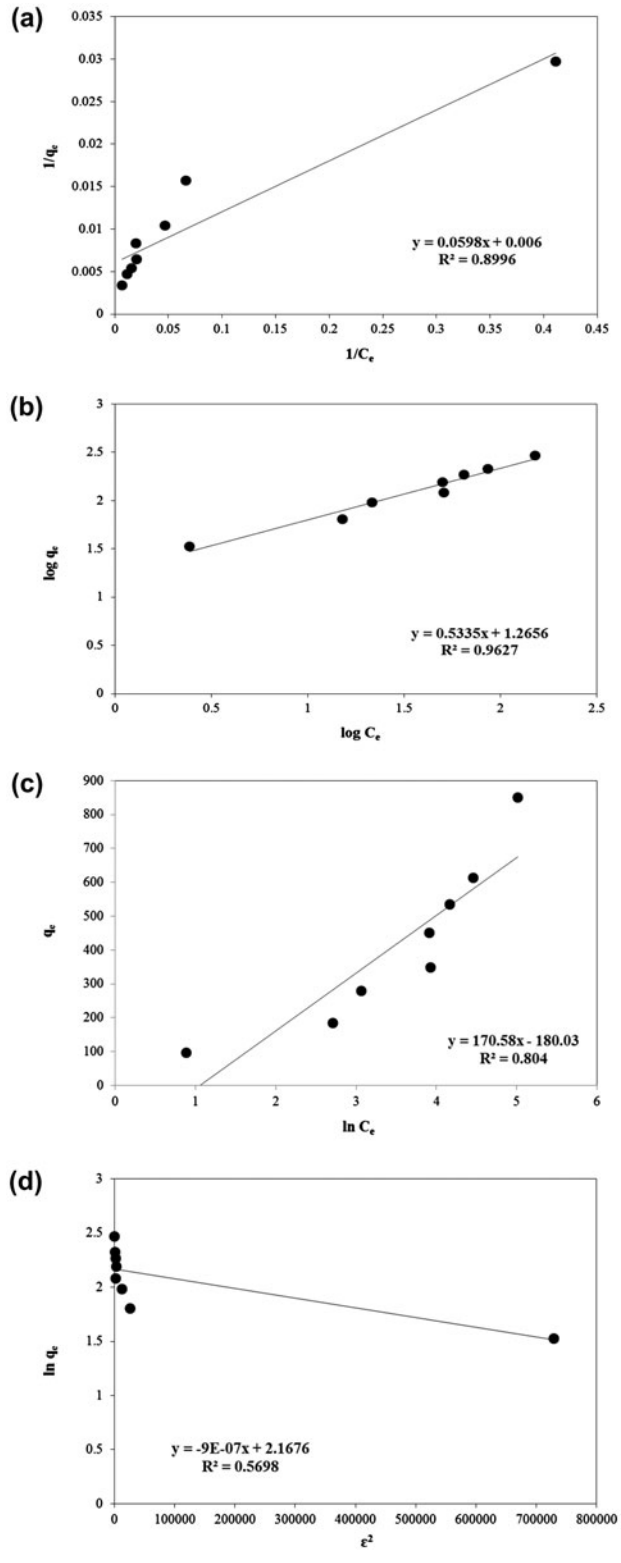

Fig. 12. Adsorption isotherms for removal of DMAZ on the activated carbon: Langmuir (a), Freundlich (b), Tempkin (c), and D–R (d).

Table 6
The adsorptive capacities of various adsorbents for DMAZ

Adsorbent	Q_m (mg/g)	Refs.
NaY zeolite	21.155	[51]
ZSM-5 zeolite	128.568	[51]
Activated carbon–commercial grade	88.028	[51]
Activated carbon-walnut shell	166.67	This study

Table 7
Kinetic parameters for pseudo-first-order, pseudo-second-order and Elovich kinetic models

	Pseudo-first-order		Pseudo-second-order		Elovich model		Intraparticle diffusion model		Experimental
Models	k_1	q_e	k_2	q_e	α	β	k_3	j	$q_{e,calc}$
Constant	0.1161	97.051	0.0059	181.818	0.0723	0.0257	18.448	56.98	181.288
R^2	0.8489		0.9993		0.834		0.6833		–

than 500 ppm, the breakthrough curve becomes steeper. Breakthrough time curve is in its equilibrium state at 500 ppm of initial DMAZ solution, while it is 6–13 min for 100–200 ppm of initial DMAZ solute, respectively.

3.7. Thermodynamic parameters

At initial DMAZ concentration of 500 ppm, the adsorbent mesh No 100 and the optimized conditions of adsorption (dosage adsorbent = 0.29 g, pH 10, agitation speed = 100 rpm, and t = 30 min), the adsorption tests were run at temperatures 15, 25, 35, and 45°C. Based on Eqs. (14) and (15) [54,55], ln K_c vs. $1/T$ was plotted (Fig. 15). Then ΔH and ΔS values were calculated from the slope and intercept of the plot. ΔG value was calculated through Eq. (16). The obtained results are tabulated in Table 8:

$$\ln K_C = \frac{\Delta S}{R} - \frac{\Delta H}{RT} \tag{14}$$

$$\frac{q_t}{C_t} = K_C \tag{15}$$

$$\Delta G = \Delta H - T\Delta S \tag{16}$$

The adsorption system of DMAZ-active carbon has positive ΔH and ΔS values (Table 8). The positive value of ΔH represents endothermic nature of the adsorption process. This fact is supported by the DMAZ adsorption increase on activated carbon and a rise in temperature. At high temperatures, active sites expand, leading to an increase in both active sites and adsorption. However, the increase of ΔH in DMAZ-activated carbon system by temperature is nearly negligible. Also, low value of ΔH indicates that the nature of the adsorption is physical. Positive value of ΔS shows more randomness of the system at solid–liquid interface during DMAZ adsorption on the activated cabon. In solution, DMAZ is surrounded with a tightly bound hydration layer where water molecules are more highly ordered than in the bulk water. When DMAZ molecule comes into close interaction with the hydration surface of carbon active, the ordered water molecules in these two hydration layers are compelled and disturbed, leads to an increase in water molecules' entropy. Although the DMAZ molecules adsorption on activated carbone decreases their freedom degree, it is possible that positive entropy associated with the DMAZ adsorption on the activated carbon be due to an increase in water molecules entropy over weighing the entropy decrease of DMAZ molecules [56–58]. Negative values of ΔG indicate that the DMAZ adsorption on activated carbon is favorable spontaneously and thermodynamically. In other words, the values of ΔG decrease by an increase in temperature, indicates more efficient adsorption at higher temperature.

Surface treatment of the walnut shell with $ZnCl_2$ (as mentioned in Section 2.1) leads to an increase in hydrophobic surface and modification of porous structures, which in turn improves adsorption capacity greatly. When the oxygen containing functional groups was removed by the heating process, the carbon surface became more hydrophobic, providing more active sites to adsorb DMAZ [59].

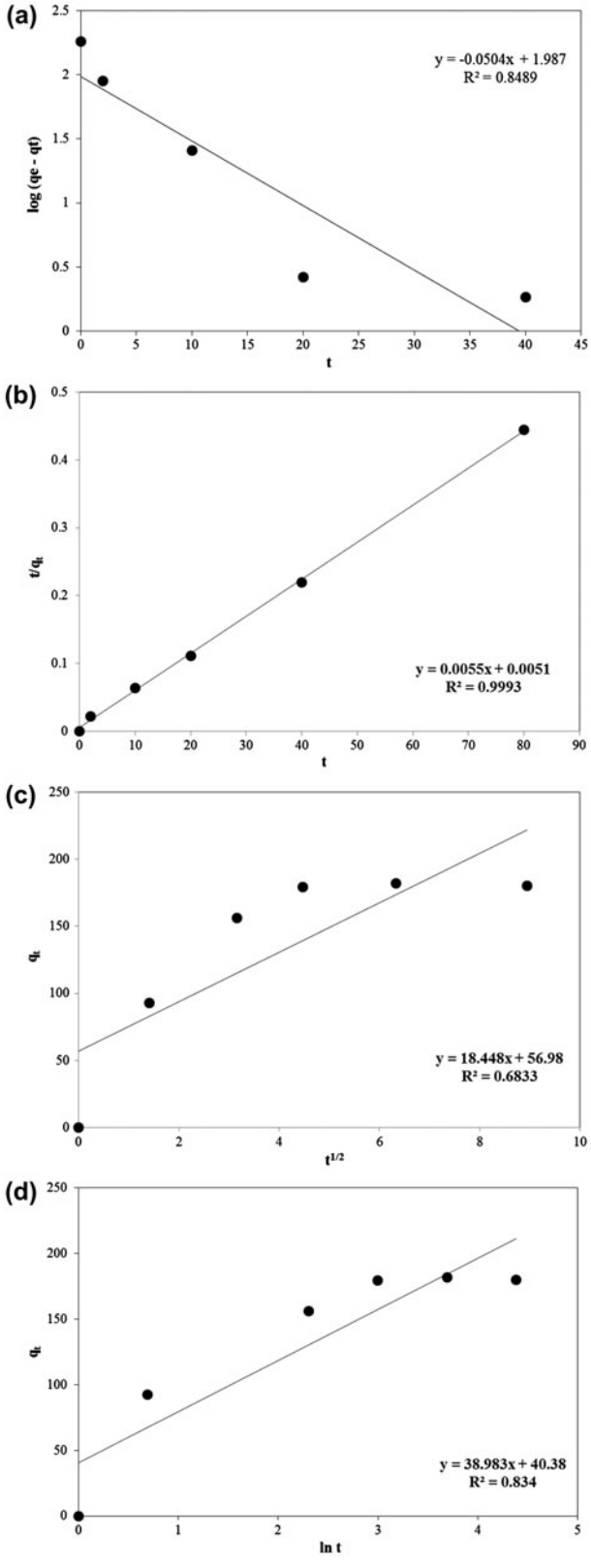

Fig. 13. Adsorption kinetics for removal of DMAZ on the activated carbon: Pseudo-first-order (a), Pseudo-second-order (b), Intraparticle diffusion (c), and Elovich (d).

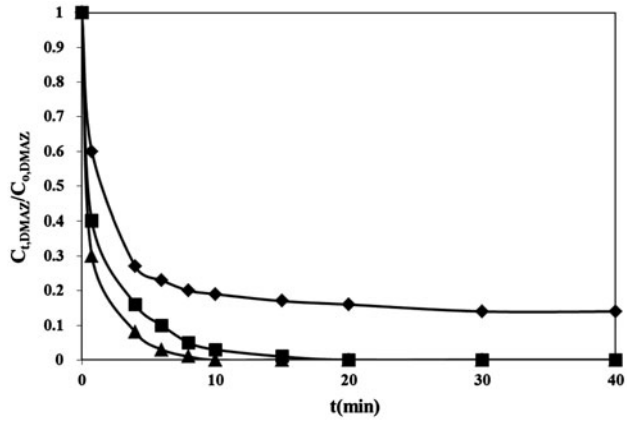

Fig. 14. Comparison of the experimental breakthrough curves obtained at pH 10, ω = 100 rpm, adsorbent dosage of 0.29 mg, and different initial concentration of DMAZ, (-♦-: $C_{0,DMAZ}$ = 500 ppm, -■-: $C_{0,DMAZ}$ = 200 ppm, -▲-: $C_{0,DMAZ}$ = 100 ppm).

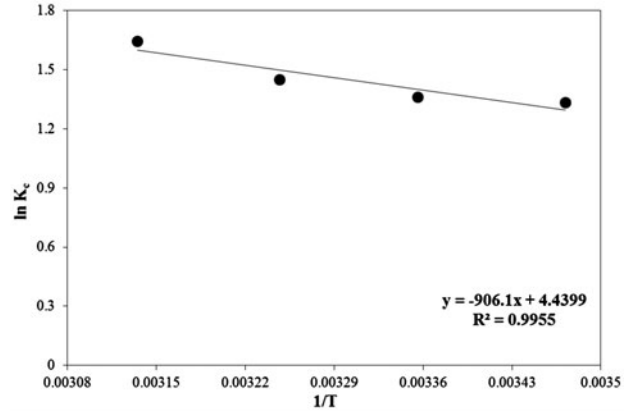

Fig. 15. Thermodynamic plot for adsorption of DMAZ on the activated carbon.

Table 8
Thermodynamic parameters for DMAZ adsorption on the activated carbon

T (K)	ΔH (kJ/mol)	ΔS (kJ/mol K)	ΔG (kJ/mol)
288	+7.539	+0.037	−3.088
298			−3.457
308			−3.826
318			−4.195

3.8. Regeneration of the adsorbent and recovery of DMAZ

Due to importance of the adsorbed DMAZ on the activated carbon, it should be recovered. For this purpose and regeneration of the adsorbent, the

Table 9
The results of DMAZ adsorption with regenerated adsorbents using different eluants

Eluants	Adsorption percentage (%)
HCl (0.1 M)	84.7
H_2SO_4 (0.1 M)	61
H_3PO_4 (0.1 M)	54

adsorbent was first poured into beakers containing different acidic eluants (like HCl, H_2SO_4, H_3PO_4); next the beakers were shaken for 8 h, and decanted; then, the adsorbents were washed with redistilled boiling water. This process was repeated for six times. Finally, the adsorbents were dried at 110˚C for 2 h. The results of adsorption process with the regenerated adsorbents indicated that eluant HCl provided the highest adsorption. The results of adsorption with regenerated adsorbents are tabulated in Table 9. In this process, the adsorbed DMAZ was neutralized by acid solution (i.e. $C_4H_{10}N_4 + HCl \rightarrow C_4H_{11}ClN_4$ or $C_4H_{10}N_4 + HCl \rightarrow C_4H_{10}N_4{\cdot}HCl$) where $C_4H_{11}ClN_4$ or $C_4H_{10}N_4{\cdot}HCl$ is the neutralized form of DMAZ, which is sent to the main DMAZ production processing unit.

4. Conclusions

DMAZ is consumed in space industries. In purification of DMAZ through pervaporation process, permeate phase (containing very low concentrations of DMAZ) is released into the environment as waste. Since the recovery of DMAZ is not economic, DMAZ was removed by adsorption on the activated carbon. The feasibility of using the activated carbon from the walnut shell for this purpose has become evident through successful attempts. The activated carbon was prepared from walnut shell with zinc chloride ($ZnCl_2$) activation. The results indicated that the adsorption capacity of the adsorbent was affected by solution pH, adsorbent dosage, and agitation speed. At initial 500 ppm concentration of DMAZ, the optimum conditions were obtained as pH 10, $\omega = 100$ rpm, and the adsorbent dosage = 0.29 g. Under the optimized conditions, the obtained removal percentage was 85.95%. The Langmuir, Freundlich, Tempkin, and D–R equations were applied express DMAZ adsorption phenomenon. The equilibrium data were well described by the Freundlich model. The pseudo-first-order, pseudo-second-order, and Elovich models were evaluated in kinetic data analysis for DMAZ adsorption on the activated carbon. The results indicated that the pseudo-second-order kinetic model provided a better correlation for the kinetic data. It can be deduced that the activated carbon from walnut shell is an appropriate adsorbent for removal of DMAZ from dilute aqueous solutions.

Nomenclature

C_o — initial concentration of adsorbate (mg/l or ppm)
$m_{adsorbent}$ — mass of adsorbent (g)
ω — agitation speed of shaker (rpm)
t — time (min)
T — temperature (K)
R — universal gas constant (8.314 J/mol K)
A_T — Tempkin isotherm equilibrium binding constant (l/mg)
b — Langmuir isotherm constant (l/mg)
Q_m — maximum monolayer coverage capacities (mg/g) in Langmuir isotherm
K_T — Tempkin isotherm constant related to heat absorption (RT/b)
C_e — concentration of liquid phase at equilibrium state (mg/l)
ε — Dubinin–Radushkevich isotherm constant equal to $RT \ln(1 + (1/C_e))$
$B_{D–R}$ — Dubinin–Radushkevich isotherm constant (mol^2/kJ^2)
q_s — theoretical isotherm monolayer saturation capacity (mg/g) in Dubinin–Radushkevich isotherm
K_F — Freundlich isotherm constant (mg/g) $(l/g)^n$ related to adsorption capacity
n — adsorption intensity in Freundlich isotherm
q_e — amount of DMAZ absorbed on the adsorbent at equilibrium per unit weight of adsorbent (mg/g)
q_t — amount of DMAZ adsorbed per unit weight of adsorbent at time t (mg/g)
$q_{e,calc}$ — calculated adsorbate concentration at equilibrium state (mg/g)
E — mean free energy (kJ/mol)
k_1 — rate constants of pseudo-first-order adsorptions kinetic equation (1/min)
k_2 — rate constants of pseudo-second-order adsorptions kinetic equation (g/mg min)
k_3 — rate constants of intraparticle diffusion adsorptions kinetic equation
j — constants of intraparticle diffusion adsorptions kinetic equation related to the thickness of the boundary layer
α — the initial adsorption rate of Elovich adsorptions kinetic equation (mg/g min)
β — adsorption constant of Elovich adsorptions kinetic equation related to the extent of the surface coverage and activation energy for chemisorption (g/mg)
ΔG — Gibbs energy change (kJ/mol)
ΔH — enthalpy change (kJ/mol)
ΔS — entropy change (kJ/mol K)

References

[1] E.W. Schmidt, Hydrazine and Its Derivatives, Wiley, New York, NY, 2001.
[2] J.P. Agrawal, High Energy Materials: Propellants, Explosives and Pyrotechnics, Wiley-VCH, Weinheim, 2010.
[3] C.J. Meyers, B.M. Kosowski, Dimethylamino ethylazide—A replacement of hydrazine derivatives in hypergolic fuel applications, Int. Annu. Conf. ICT 177 (2003) 1–4.
[4] D.M. Thompson, Tertiary Amine Azides in Hypergolic Liquid or Gel Fuels Propellant Systems, US Patent 6013143, 2000.
[5] G. Reddy, J. Song, M.S. Mecchi, M.S. Johnson, Genotoxicity assessment of two hypergolic energetic propellant compounds, Mutat. Res. Genet. Toxicol. Environ. Mutagen. 700 (2010) 26–31.
[6] B. Mellor, A preliminary technical review of DMAZ: A low toxicity hypergolic fuel, in: 2nd International Conference on Green Propellants for Space Propulsion, European Space Agency, Italy, 2004, pp. 967–986.
[7] P. Schiemenz, H. Engelhard, Trimethoxyphenylverbindungen, I. Synthese von Aminoamiden über gemischte Anhydride, Chem. Ber. 92 (1959) 857–862.
[8] S.G. Pakdehi, S. Sobhani, I. Kohsari, A kinetic study on synthesis of liquid fuel dimethyl amino ethyl azide (DMAZ), J. Energy Mater. 9 (2009) 45–50.
[9] K. Shafiei, DMAZ Dewatering Via Zeolite Membrane, PhD Thesis, Iran University of Science & Technology, Tehran, 2014.
[10] S.G. Pakdehi, T. Mohammadi, K. Shafiei, M. Kazemimoghaddam, Study on zeolite membranes for dehydration of DMAZ, J. Energy Mater. 3 (2013) 23–35.
[11] F. Rezaei, A Thermo-Kinetic Study on DMAZ Adsorption from Dilute Solution by a Cheap Plant Adsorbent, MSc Thesis, Malek Ashtar University of Technology, Tehran, 2015.
[12] H. Feather, A remarkable adsorbent for dye removal, in: J. Mittal, A. Mittal, Chapter 11 of the Book "Green Chemistry for Dyes Removal from Wastewater", 2015, pp. 409–857 by S.K. Sharma Dr (Eds.), Scrivener Publishing LLC, USA (ISBN: 978-1-118-72099-8).
[13] A.A. Lewinsky, Hazardous Materials and Wastewater Treatment, Removal and Analysis, Nova Science Publisher, New York, NY, 2007.
[14] S.M. Alshehri, M. Naushad, T. Ahamad, Z.A. Al-Othman, A. Aldalbahi, Synthesis, characterization of curcumin based ecofriendly antimicrobial bioadsorbent for the removal of phenol from aqueous medium, Chem. Eng. J. 254 (2014) 181–189.
[15] M. Naushad, Z.A. Al-Othman, M.R. Awual, M.M. Alam, G.E. Eldesoky, Adsorption kinetics, isotherms, and thermodynamic studies for the adsorption of Pb^{2+} and Hg^{2+} metal ions from aqueous medium using Ti(IV) iodovanadate cation exchanger, Ionics 21 (2015) 2237–2245.
[16] M.R. Khan, M.A. Khan, Z.A. Al-Othman, I.H. Al-Sohaimi, M. Naushad, N.H. Al-Shaalan, Quantitative determination of methylene blue in environmental samples by solid-phase extraction and ultra-performance liquid chromatography-tandem mass spectrometry: A green approach, RSC Adv. 4 (2014) 34037–34044.
[17] M. Naushad, Z.A. Al-Othman, M.R. Khan, N.J. Al-Qahtani, I.H. Al-Sohaimi, Equilibrium, kinetics and thermodynamic studies for the removal of organophosphorus pesticide using Amberlyst-15 resin: Quantitative analysis by liquid chromatography–mass spectrometry, J. Ind. Eng. Chem. 20 (2014) 4393–4400.
[18] G. Sharma, M. Naushad, A. Kumar, S. Devi, M.R. Khan, Lanthanum/cadmium/polyaniline bimetallic nanocomposite for the photodegradation of organic pollutant, Iran. Polym. J. 24 (2015) 1003–1013.
[19] M.R. Awual, M.M. Hasan, A. Shahat, M. Naushad, H. Shiwaku, T. Yaita, Investigation of ligand immobilized nano-composite adsorbent for efficient cerium(III) detection and recovery, Chem. Eng. J. 265 (2015) 210–218.
[20] A. Kumar, G. Sharma, M. Naushad, P. Singh, S. Kalia, Polyacrylamide/$Ni_{0.02}Zn_{0.98}O$ nanocomposite with high solar light photocatalytic activity and efficient adsorption capacity for toxic dye removal, Ind. Eng. Chem. Res. 53 (2014) 15549–15560.
[21] V.K. Gupta, A. Mittal, R. Jain, M. Mathur, S. Sikarwar, Adsorption of Safranin-T from wastewater using waste materials—Activated carbon and activated rice husks, J. Colloid Interface Sci. 303 (2006) 80–86.
[22] M. Naushad, M.R. Khan, Z.A. Al-Othman, I. Al-Sohaimi, F. Rodriguez-Reinoso, T.M. Turki, R. Ali, Removal of Br $O3^{-}$ from drinking water samples using newly developed agricultural waste-based activated carbon and its determination by ultra-performance liquid chromatography-mass spectrometry, Environ. Sci. Pollut. Res. 22 (2015) 15853–15865.
[23] M.M. Yeganeh, T. Kaghazchi, M. Soleimani, Effect of raw materials on properties of activated carbons, Chem. Eng. Technol. 29 (2006) 1247–1251.
[24] A. Mittal, V. Thakur, J. Mittal, H. Vardhan, Process development for the removal of hazardous anionic azo dye Congo red from wastewater by using hen feather as potential adsorbent, Desalin. Water Treat. 52 (2014) 227–237.
[25] M.S. Balathanigaimani, H.C. Kang, W.G. Shim, C. Kim, J.W. Lee, H. Moon, Preparation of powdered activated carbon from rice husk and its methane adsorption properties, Korean J. Chem. Eng. 23 (2006) 663–668.
[26] C. Srinivasakannan, M.Z. Abu Bakar, Production of activated carbon from rubber wood sawdust, Biomass Bioenergy 27 (2004) 89–96.
[27] A. Mittal, L. Krishnan, V.K. Gupta, Removal and recovery of malachite green from wastewater using an agricultural waste material, de-oiled soya, Sep. Purif. Technol. 43 (2005) 125–133.
[28] M. Sulaiman, M. Ismail, A. Jusoh, Oil-palm shell activated carbon production using CO_2 emission from $CaCO_3$, J. Sustainability Sci. Manage. 8 (2013) 150–160.
[29] C. Namasivayam, D. Kavitha, Removal of Congo red from water by adsorption onto activated carbon prepared from coir pith, an agricultural solid waste, Dyes Pigm. 54 (2002) 47–58.
[30] A. Mittal, R. Jain, J. Mittal, M. Shrivastava, Adsorptive removal of hazardous dye quinoline yellow from waste water using coconut-husk as potential adsorbent, Fresenius Environ. Bull. 19 (2010) 1–9.
[31] V.K. Gupta, A. Mittal, D. Jhare, J. Mittal, Batch and bulk removal of hazardous colouring agent Rose Bengal by adsorption techniques using bottom ash as adsorbent, RSC Adv. 2 (2012) 8381–8389.

[32] D. Montgomery, Design and Analysis of Experiments, John Wiley & Sons Inc., New Jersey, NJ, 2013.
[33] A. Mittal, L. Kurup, J. Mittal, Freundlich and Langmuir adsorption isotherms and kinetics for the removal of Tartrazine from aqueous solutions using hen feathers, J. Hazard. Mater. 146 (2007) 243–248.
[34] I. Langmuir, The constitution and fundamental properties of solids and liquids. Part I. Solids, J. Am. Chem. Soc. 38 (1916) 2221–2295.
[35] H.M.F. Freundlich, Uber die adsorption in losungen, Z. Phys. Chem. 57 (1906) 385–470.
[36] K.W. Kolasniski, Surface Science, Wiley, Chichester, 2001.
[37] C. Nguyen, D.D. Do, The Dubinin–Radushkevich equation and the underlying microscopic adsorption description, Carbon 39 (2001) 1327–1336.
[38] S. Lagergren, Zur theorie der sogenannten adsorption geloster stoffe, Handlingar 24 (1898) 1–39.
[39] W. Rudzinski, W. Plazinski, Kinetics of solute adsorption at solid/solution interfaces: A theoretical development of the empirical pseudo-first and pseudo-second-order kinetic rate equations, based on applying the statistical rate theory of interfacial transport, J. Phys. Chem. B 110 (2006) 16514–16525.
[40] S. Azizian, Kinetic models of sorption: A theoretical analysis, J. Colloid Interface Sci. 276 (2004) 47–52.
[41] S.H. Chien, W.R. Clayton, Application of Elovich equation to the kinetics of phosphate release and sorption in soils, Soil Sci. Soc. Am. J. 44 (1980) 265–268.
[42] F. Grant, Design-Expert 7.1 Software Review, Scientific Computing World, New York, NY, 2007.
[43] A.R. Yari, M.S. Siboni, S. Hashemi, M. Alizadeh, Removal of heavy metals from aqueous solutions by natural adsorbents: A review, Arch. Hyg. Sci. 2 (2013) 114–124.
[44] D.S. Thambavani, B. Kavitha, Removal of chromium (VI) ions by adsorption using river bed sand from Tamilnadu—A kinetic Study, Int. J. Res. 1 (2014) 718–742.
[45] A. Gholizadeh, M. Kermani, M. Gholami, M. Farzadkia, K. Yaghmaeian, Removal efficiency, adsorption kinetics and isotherms of phenolic compounds from aqueous solution using rice bran ash, Asian J. Chem. 25 (2013) 3871–3878.
[46] A. Mittal, D. Jhare, J. Mittal, Adsorption of hazardous dye Eosin Yellow from aqueous solution onto waste material De-oiled Soya: Isotherm, kinetics and bulk removal, J. Mol. Liq. 179 (2013) 133–140.
[47] F. Mikati, M. El Jamal, Biosorption of methylene blue on chemically modified chaetophora elegans algae by carboxylic acid, J. Sci. Ind. Res. 72 (2013) 428–434.
[48] M. Tsezos, J.P. Bell, A mechanistic study on the fate of malathion following interaction with microbial biomass, Water Res. 25 (1991) 1039–1046.
[49] H. Daraei, A. Mittal, M. Noorisepehr, J. Mittal, Separation of chromium from water samples using eggshell powder as a low-cost sorbent: Kinetic and thermodynamic studies, Desalin. Water Treat. 53 (2015) 214–220.
[50] K.H. Foo, B.H. Hameed, Insights into the modeling of adsorption isotherm systems, Chem. Eng. J. 156 (2010) 2–10.
[51] S.G. Pakdehi, B. Vaferi, A study on adsorptive removal of DMAZ from aqueous solutions by ZSM-5, NaY zeolites, and activated carbon: Kinetic and isotherm, 2015 Desalin. Water Treat. 1–7 doi: 10.1080/19443994.2015.1091748.
[52] Z. Aksu, F. Gonen, Biosorption of phenol by immobilized activated sludge in a continuous packed bed: Prediction of breakthrough curves, Process Biochem. 39 (2004) 599–613.
[53] J.P. Chen, X. Wang, Removing copper, zinc, and lead ion by granular activated carbon in pretreated fixed bed columns, Sep. Purif. Technol. 19 (2000) 157–167.
[54] A.K. Bhattacharya, T.K. Naiya, S.N. Mandal, S.K. Das, Adsorption, kinetics and equilibrium studies on removal of Cr(VI) from aqueous solutions using different low-cost adsorbents, Chem. Eng. J. 137 (2008) 529–541.
[55] B. Singha, S.K. Das, Removal of Pb(II) ions from aqueous solution and industrial effluent using natural biosorbents, Environ. Sci. Pollut. Res. 19 (2012) 2212–2226.
[56] G.D. Sheng, D.D. Shao, X.M. Ren, X.Q. Wang, J.X. Li, Y.X. Chen, X.K. Wang, Kinetics and thermodynamics of adsorption of ionizable aromatic compounds from aqueous solutions by as-prepared and oxidized multiwalled carbon nanotubes, J. Hazard. Mater. 178 (2010) 505–516.
[57] J. Hu, D. Shao, C. Chen, G. Sheng, X. Ren, X. Wang, Removal of 1-naphthylamine from aqueous solution by multiwall carbon nanotubes/iron oxides/cyclodextrin composite, J. Hazard. Mater. 185 (2011) 463–471.
[58] M.M. Li, H.C. Pan, S.L. Huang, M. Scholz, Controlled experimental study on removing diesel oil spillages using agricultural waste products, Chem. Eng. Technol. 36 (2013) 673–680.
[59] P. Serp, B. Machado, Nanostructured Carbon Materials for Catalysis, Royal Society of Chemistry, Cambridge, 2015.